B4

by Rahadi Wirawan

Submission date: 22-Feb-2022 07:09AM (UTC+0700)
Submission ID: 1767881795
File name: Lamp._B4.pdf (611.54K)
Word count: 4521
Character count: 22876

Applied Radiation and Isotopes 155 (2020) 108924

Contents lists available at ScienceDirect

Applied Radiation and Isotopes

journal homepage: http://www.elsevier.com/locate/apradiso

Gamma backscattering analysis of flaw types and orientation based on Monte Carlo GEANT4 simulations

R. Wirawan [a,*], L.M. Angraini [a], N. Qomariyah [a], A. Waris [b], M. Djamal [b]

[a] Department of Physics, FMIPA, University of Mataram, Jl. Majapahit 62, Mataram, 83125, Indonesia
[b] Department of Physics, FMIPA, Institut Teknologi Bandung, Jl. Ganesha 10, Bandung, 40132, Indonesia

ARTICLE INFO

Keywords:
^{137}Cs source
Duralumin
Monte Carlo simulation
Orientation
Slit

ABSTRACT

In this study, we modeled the effects of flaws in a solid material as three different slit types (rectangular, rectilinear, and semicircular) and their orientations in a duralumin (aluminum alloy) plate in simulations based on 137Cs gamma backscattering. The simulations were performed using the Monte Carlo GEANT4 simulation toolkit. The simulation results showed that the shape of the slit had a small effect on the backscattering peak curve. Rotating the slit on the Y-axis and Z-axis of the duralumin plate influenced the 137Cs backscattering peak height in the energy range from 0.185 to 0.20 MeV, where the backscattering peak areas exhibited specific patterns due to the slit orientations.

1. Introduction

Flaws are the most common problems that affect solid materials, where they can be both visible and invisible, and present in forms such as a density anomaly, cavity, crack or slit. The presence of flaws in materials can reduce the mechanical strength and affect their electrical properties. The gamma backscattering technique (GBT) can be employed to investigate invisible flaws located inside or on the back of high density materials. GBT is a non-destructive test based on the use of gamma penetrating radiation for determining the characteristics of test materials by analyzing the scattering energy spectra captured by the detector. Several studies have reported the use of GBT in application such as determining the local density perturbation (Boldo and Appoloni, 2014), concrete thickness (Almayahi, 2015), effective atomic number (Kiran et al., 2015; Sharma et al., 2017; Hosamani and Badiger, 2018), wood density (Tondon et al., 2017), and saturation depth (Nguyen et al., 2018).

Computer simulations can be conducted in the early stages when studying the characteristics of flaws, which can be achieved using a Monte Carlo (MC) numerical simulation application. This type of simulation has been applied widely. Studies have shown that MC simulations can be employed successfully for the optimization of a detector collimator (Tavakoli-Anbaran et al., 2009), studying the performance of detectors (Peeples and Gardner, 2012), examining source distributions (Gurau and Sima, 2012), determining the concentrations of low-Z solutions (Priyada et al., 2012), evaluating voids in concrete (Priyada et al., 2013), investigating multiple backscattering on a target (Tarim et al., 2013), and improving the accuracy of a nuclear densitometer (Golgun et al., 2016). In addition, MC simulations have been conducted to determine the backscattered gamma energy distributions for metallic, biological, and shielding materials (Aydın, 2018).

During scattering interactions, the presence of flaws in a material will reduce the material's volume and also affect the number of electrons that might interact with a gamma photon, thereby influencing the characteristic backscattering curve detected for the energy spectrum distribution. In addition, the shape and orientation of the flaws can potentially influence the scattering direction and scattering path of a photon when passing through a material. Studies are required in order to understand the significant characteristic of these effects on the backscattering peak curve and to develop a non-destructive testing system.

In the present study, we investigated the effects on the gamma backscattering peak characteristics of different flaw types and their orientations located on the bottom of a duralumin (aluminum alloy) plate surface. This study was conducted using the GEANT4-MC simulation approach.

2. Theoretical background

The gamma photons detected when investigating the presence of flaws comprise the direct gamma-rays from a gamma source and indirect

* Corresponding author.
E-mail address: rwirawan@unram.ac.id (R. Wirawan).

https://doi.org/10.1016/j.apradiso.2019.108924
Received 1 November 2018; Received in revised form 15 September 2019; Accepted 2 October 2019
Available online 3 October 2019
0969-8043/

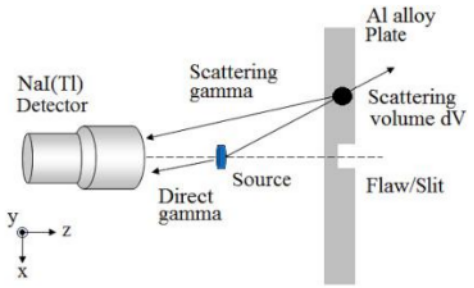

Fig. 1. Geometrical setup of the gamma interaction simulation.

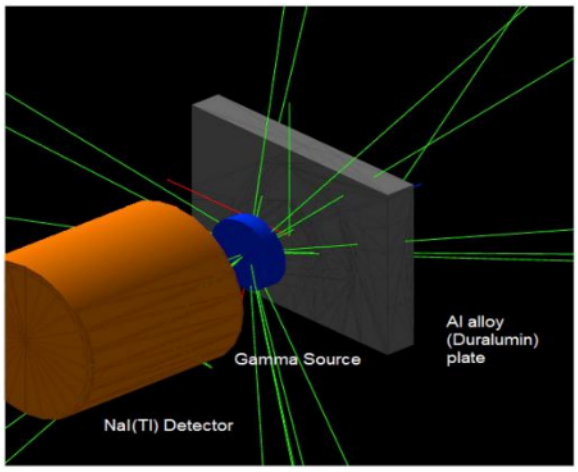

Fig. 2. GEANT4 visualization simulation setup for detecting backscattering gamma-rays from a duralumin (aluminum alloy) plate.

gamma-rays due to scattering by a plate, as shown in Fig. 1. The attenuation of gamma photons from the source to a detector is described using the Beer–Lambert formula:

$$I = I_s(E)\exp\left[-\sum\left(\frac{\mu(E)}{\rho}\right)_i \rho_i r_i\right], \quad (1)$$

where $I_s(E)$ is the intensity of the gamma source, ρ is the density of the plate material, $\left(\frac{\mu(E)}{\rho}\right)$ is the mass absorption coefficient, and r is the photon movement path.

According to the single scattering model (Ball et al., 1998), photons undergo attenuation before interacting with matter. They are then scattered by the scattering matrix volume and attenuated when the photon moves toward the detector. This scattering involves electron–electron interactions via the Compton scattering mechanism. The number of electrons can be determined based on the electron density n in the following relationship:

$$n = Z\frac{N_A\rho}{A}, \quad (2)$$

where Z is the atomic number, N_A is Avogadro's number, ρ is the density of the material, and A is the atomic mass. Photons will be deflected at a certain angle and scattering energy. The distribution of scattered photons is described by the differential cross-section per solid angle ($d\sigma/d\Omega$) with the Klein–Nishina formula (Knoll, 1989):

$$\frac{d\sigma}{d\Omega} = \frac{Zr_0^2}{2}(1+\cos^2\theta)\left(\frac{1}{1+\alpha(1-\cos\theta)}\right)^2\left(1+\frac{\alpha^2(1-\cos\theta)^2}{(1+\alpha(1-\cos\theta))(1+\cos^2\theta)}\right), \quad (3)$$

where $\alpha = E/m_0c^2$, r_0 is the classical electron radius (2.82 fm), and θ is the scattered photon angle.

The scattering intensity of a detected gamma photon can be obtained using equation (4):

$$I_{scatt} = \int I_s(E)\exp\left[-\sum\left(\frac{\mu(E)}{\rho}\right)_i \rho_i r_i\right] x \left(Z\frac{N_A\rho}{A}\right) x \left(\frac{d\sigma}{d\Omega}\right) d\Omega\ dV, \quad (4)$$

where dV is the scattering volume element of the plate, $d\Omega$ is the solid angle, and $I_s(E)$ is the source intensity. The total intensity detected by the detector comprises the direct intensity from the source and the indirect intensity from scattering interactions, as summarized in equation (5).

$$I = I_s(E)\exp\left[-\sum\left(\frac{\mu(E)}{\rho}\right)_i \rho_i r_i\right] + \int I_s(E)\exp\left[-\sum\left(\frac{\mu(E)}{\rho}\right)_i \rho_i r_i\right] x \left(Z\frac{N_A\rho}{A}\right) x \left(\frac{d\sigma}{d\Omega}\right) d\Omega\ dV, \quad (5)$$

The volume element parameter can influence the scattered photon intensities detected by a detector. Therefore, reducing the volume element from the solid material (plate) will affect the intensity of the detected photons. In this study, the number of photons detected was traced using the MC GEANT4 simulation approach in the form of an energy distribution spectrum curve.

3. GEANT4 simulation

In order to obtain gamma-ray scattering intensity data, the simulation was conducted using the GEANT4 (GEometry ANd Tracking) MC simulation toolkit, which is an object-oriented program (Agostinelli et al., 2003). A schematic showing the design of the backscattering gamma simulation is depicted in Fig. 2. The duralumin (aluminum alloy) plate material comprised Al = 94.55%, Cu = 4.36%, and Mg = 1.09% according to energy-dispersive X-ray spectroscopy analysis (Wirawan et al., 2017) and using the density formulation for a mixed material given in equation (6):

$$\rho_{Al\ alloy} = \frac{\rho_{Mg}V_{Mg} + \rho_{Al}V_{Al} + \rho_{Cu}V_{Cu}}{V_{Mg} + V_{Al} + V_{Cu}}, \quad (6)$$

where the density (ρ) value was about 2.77 g/cm^3. As shown in Fig. 2, a duralumin plate (dimensions: 8.0 cm × 6.0 cm × 1.0 cm) and ^{137}Cs gamma source were placed 4.3 cm and 1.55 cm from the detector's surface, respectively. The detector model used in the simulation was a scintillation detector with cylindrical NaI(Tl) measuring 5.08 cm × 5.08 cm as the sensitive material. According to the model of Shi et al. (2002), the NaI(Tl) was covered by MgO, SiO_2, and Al layers with thicknesses of 0.185 cm, 0.3 cm, and 0.05 cm, respectively.

The gamma-ray source model considered in the simulation was an encapsulated point source comprising an acrylic (polymethyl methacrylate ($C_5H_8O_2$) with a density of 1.18 g/cm^3) disk model with a diameter of 2.5 cm and thickness of 0.5 cm. The physical processes used in the simulation was "/physics/addPhysics empenelope" and "/physics/setCuts 0.01 mm" was set for producing cuts of secondary particles. The simulation was performed for 5.0 × 10^7 beamOns (histories).

The smearing process was performed for the histogram output obtained from GEANT4 in order to create a spectrum curve for the energy distribution in 300 bins. The energy resolution of the NaI(Tl) detector used for smearing was 8.6%. The backscattering peaks of the gamma-rays were analyzed based on a Gaussian function and Chi-square method for the fitted settings. The smearing process and analysis was conducted using the ROOT C/C ++ program.

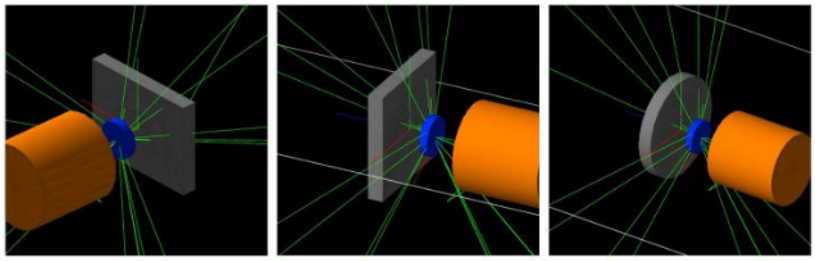

Fig. 3. Visualizations of the geometry for the three types of plates using GEANT4: (a) rectangular, (b) rectilinear, and (c) disk.

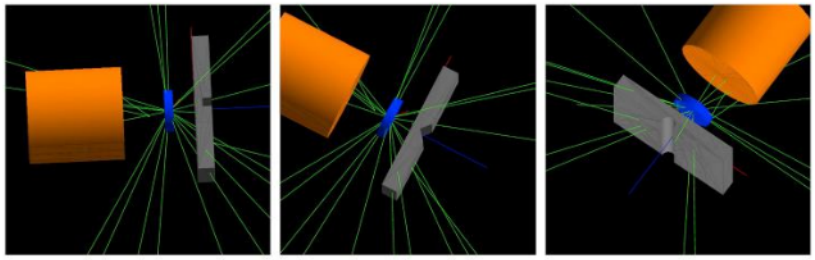

Fig. 4. Visualizations of different types of slit with GEANT4.

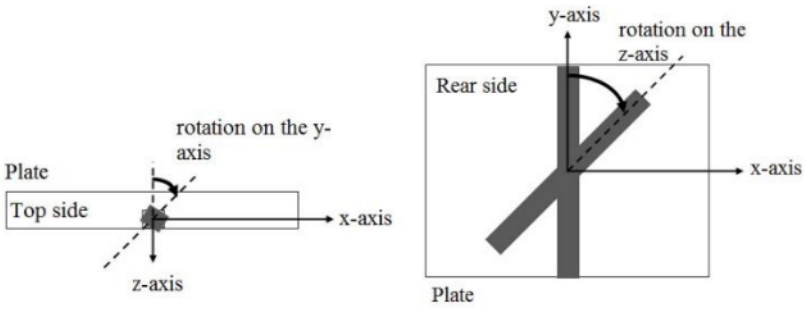

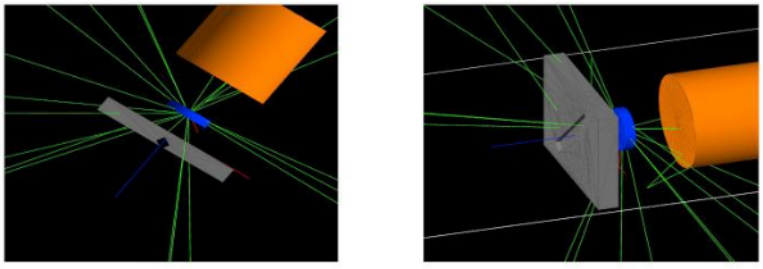

Fig. 5. Different slit orientations.

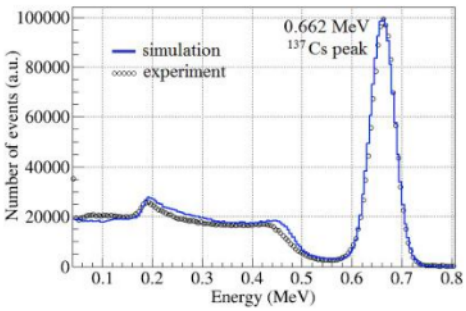

Fig. 6. Simulated and experimental energy spectrum distributions for the ^{137}Cs gamma source.

3.1. Construction of plate and flaw geometry

In order to study the influence of the geometry of the plate, we simulated three types of plate with the same volume (Fig. 3), i.e., rectangular (dimensions: 8.0 cm × 6.0 cm × 1.0 cm), rectilinear (6.93 cm × 6.93 cm × 1.0 cm), and a disk (radius = 3.91 cm radius and thickness = 1 cm).

In order to determine the effect of the presence of a flaw/slit on the gamma backscattering spectrum, we simulated the presence of three types of slit on the bottom of the duralumin plate, as shown in Fig. 4. The slit types were rectangular (0.6 cm × 6.0 cm × 0.5 cm), triangular (1.2 cm × 6.0 cm × 0.5 cm), and semicircular (radius = 0.437 cm and height = 6.0 cm), and they all had the same volume.

3.2. Construction of slit orientation

Furthermore, in order to study the characteristics of the backscattering peak for ^{137}Cs gamma depending on the slit orientation, we simulated slit orientations perpendicular (Y-axis) and parallel to the normal plate surface (Z-axis), as depicted in Fig. 5. The slit type considered in this study was rectangular with dimensions of 0.6 cm × 6.0 cm × 0.5 cm.

Due to the presence of a slit/crack and its orientation, the backscattering peak was analyzed, i.e., the peak curve height and peak area of the backscattering curve. The backscattering peak height was determined based on a Gaussian fitted curve and the characteristics of the Gaussian curve. In addition, the area (A) below the peak was determined using the following formula (Knoll, 1989).

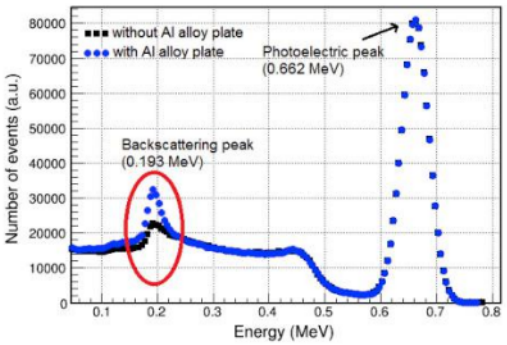

(a) Energy spectrum distribution

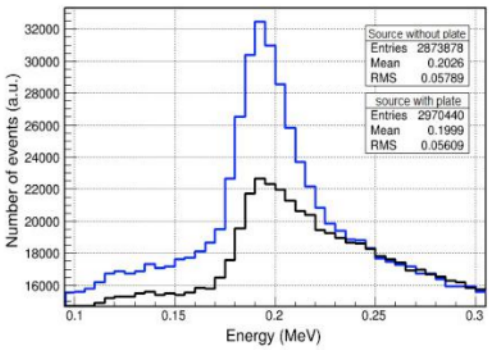

(b) Backscattering peak

Fig. 7. Energy spectrum distribution for the ^{137}Cs gamma source with and without the Al alloy plate.

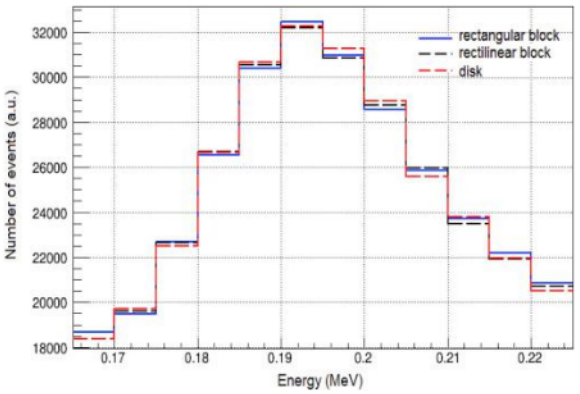

Fig. 8. Backscattering peak curves obtained for ^{137}Cs gamma-rays.

$$A = \sqrt{2\pi}\,\sigma\, y_0 = 2.507\sigma\, y_0, \tag{7}$$

The full-width at half maximum (*FWHM*) was evaluated using the following formula:

$$FWHM = 2\sqrt{2\ln 2}\,\sigma = 2.355\,\sigma, \tag{8}$$

where y_o is the maximum height of the curve's peak and σ is the standard deviation. The resolution (R) of the *FWHM* can be determined using the following equation:

$$R(\%) = \frac{FWHM}{H_0} \times 100, \tag{9}$$

Table 1
Gaussian fit analyses of three types of duralumin (aluminum alloy) plate.

Plate type	Entries (photons detected)	Parameter	Value	Error
Rectangular block	2970440	Height	3.24488×10^{4}	1.79301×10^{2}
		Energy	1.92905×10^{-1}	1.87862×10^{-4}
		Sigma	1.49877×10^{-2}	9.24312×10^{-4}
Rectilinear block	2970607	Height	3.21878×10^{4}	1.79082×10^{2}
		Energy	1.92750×10^{-1}	2.15362×10^{-4}
		Sigma	1.62202×10^{-2}	1.17440×10^{-4}
Disk	2969772	Height	3.22524×10^{4}	1.25248×10^{2}
		Energy	1.93734×10^{-1}	1.36750×10^{-4}
		Sigma	1.84014×10^{-2}	3.88890×10^{-4}

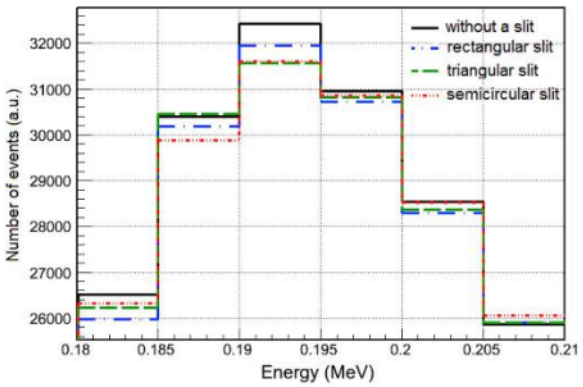

Fig. 9. Backscattering peaks obtained using the plate without and with a slit.

where H_o is the centroid of the curve's peak.

A Chi-square test was performed to determine the significance of the differences in the gamma backscattering peaks for the three types of modeled slit.

4. Results and discussion

The simulation approach for experimental testing was conducted after testing the detector's performance, including the detector's response function to the radiation from a source. Fig. 6 shows a graph of the source energy spectrum obtained from the ^{137}Cs gamma source simulation results and the source radiation measurements for the 5-μCi source's activity for 5 min. The upscaling ratio used for the simulation was about 1.23. Based on the Gaussian curve fitting results for the main peak (0.662 MeV), the *FWHM* value for the simulation was 0.05857 and the resolution (R) was 8.8565%. In addition, the *FWHM* value for the experimental curve was 0.057425 with a resolution (R) of 8.6801%.

According to the resolution of the main peak, the difference in resolution between the simulated and experimental values was about 2.03%. These results indicate that the detector model designed for obtaining measurements could produce an energy distribution curve similar to that obtained in experiments.

The effect of the presence of the duralumin plate in front of the ^{137}Cs gamma source was assessed based on the increase in the height of the backscattering peak in the gamma-ray scattering spectrum, as shown in Fig. 7a. After 5.0×10^7 beamOns from the gamma photon source, the photon number that entered the scintillation detector was about 2873878 (5.75%) in the absence of the duralumin plate.

However, when the duralumin plate was present, the photon number increased by 0.19% to 2970440 (5.94%), as shown in Fig. 7a. These additional photons were due to photons interacting with electrons in the aluminum alloy, which led to their deflection and attenuation when they moved toward the detector. The photon intensity contributed to the increase in the backscattering peak curve in the gamma energy spectrum distribution, as depicted in Fig. 7b. The change in the height of the backscattering peak due to the presence of the plate had the same pattern as that obtained experimentally by Sharma et al. (2017) when determining the effective atomic number using a ^{22}Na gamma source.

Moreover, the plate geometry influenced the backscattering peak in the energy spectrum for gamma scattering. Simulations of the different types of plates showed that the numbers of photons entering the detector when the plate comprised a rectangular block, rectilinear block, and disk were 2970440 (5.940%), 2970607 (5.941%), and 2969772 (5.939%), respectively. According to these results, the plate type influenced the number of photon entries. The heights of the backscattering peaks are shown in Fig. 8.

According to the Gaussian curves fitted for the backscattering peaks (as shown in Table 1), the rectangular block plate type obtained a higher curve height than the other two plate types. The ratios of the backscattering peak height relative to the number of photon entries were 1.092%, 1.086%, and 1.084% for the rectangular block, rectilinear block, and disk, respectively. The scattering interactions and attenuation of photons throughout the material accounted for the differences in the backscattering peak heights.

Table 2
Gaussian fit analyses of duralumin (aluminum alloy) plate without a slit and with certain types of slit.

Plate	Entries (photons detected)	Parameter	Value	Error
Duralumin plate without a slit (8.0 cm × 6.0 cm × 1.0 cm)	2970440	Height	3.24488×10^4	1.79301×10^2
		Energy	1.92905×10^{-1}	1.87862×10^{-4}
		Sigma	1.49877×10^{-2}	9.24312×10^{-4}
Duralumin plate with a rectangular slit (0.6 cm × 6.0 cm × 0.5 cm)	2966160	Height	3.19502×10^4	1.31383×10^2
		Energy	1.92952×10^{-1}	2.23163×10^{-4}
		Sigma	1.62426×10^{-2}	4.98395×10^{-4}
Duralumin plate with a triangular slit (1.2 cm × 6.0 cm × 0.5 cm)	2966302	Height	3.15042×10^4	1.04053×10^2
		Energy	1.94316×10^{-1}	1.03424×10^{-4}
		Sigma	2.01446×10^{-2}	2.21284×10^{-4}
Duralumin plate with a semicircular slit (radius = 0.437 cm; height = 6.0 cm)	2965817	Height	3.15932×10^4	1.23661×10^2
		Energy	1.93868×10^{-1}	1.47184×10^{-4}
		Sigma	1.88921×10^{-2}	4.24362×10^{-4}

Table 3
Chi-square analysis of the backscattering peaks obtained with three types of slits.

Energy Range	Histogram height				$(f_{ij} - E_{ij})^2 / E_{ij}$			
	Rectangular slit	Triangular slit	Semicircular slit	Σ	Rectangular slit	Triangular slit	Semicircular slit	Σ
0.180–0.185	25993.6	26234.9	26334.7	78563.2	1.0614	0.0284	0.7412	1.831
0.185–0.190	30206.7	30465.9	29904	90576.6	0.0708	2.0816	2.9206	5.073
0.190–0.195	31949.4	31561.8	31607.8	95119.0	2.4114	0.8958	0.3662	3.6734
0.195–0.200	30723.5	30832.6	30854.4	92410.5	0.0738	0.0011	0.0571	0.132
0.200–0.205	28297	28378.6	28537	85212.6	0.211	0.0782	0.5458	0.835
0.205–0.210	25902.8	25912.6	26067.5	77882.9	0.0368	0.1783	0.3772	0.5923
Σ	173073	173386.4	173305.4	519764.8	Chi-square (χ^2) value			12.137

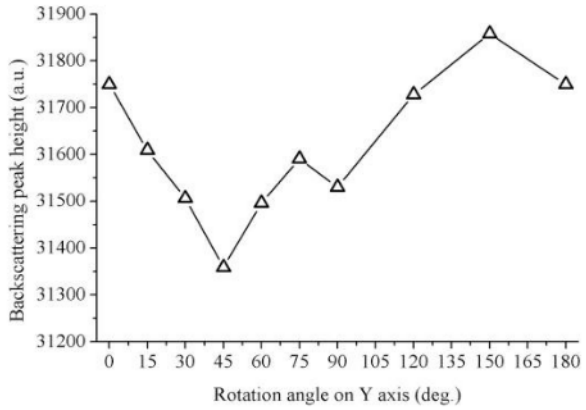

Fig. 10. Heights of ^{137}Cs gamma backscattering peaks with different rotational angles on the Y-axis for a rectangular plate of duralumin (aluminum alloy).

The presence of a slit under the duralumin plates influenced the backscattering peak in the gamma energy distribution for the ^{137}Cs source. Fig. 9 show the backscattering peaks obtained for a plate without a slit and plates with the three different types of slits presented in Fig. 4. The different slit types yielded different numbers of photon entries. The slits had the same volume but the shape of each slit affected the number of photons that entered the detector. The presence of a slit reduced the height of the backscattering peak compared with that in the absence of a slit. The decrease in the backscattering peak for the ^{137}Cs gamma-ray scattering was due to the reduced volume of the scattering plate (or slit volume). Thus, there was a decrease in the number of electrons that probably interacted with gamma photons from the ^{137}Cs source. The reduced volumes also affected the attenuation of the scattered photon intensity when photons passed through the duralumin plate.

The Gaussian curves fitted to the gamma backscattering peaks obtained for the three slit types showed that the rectangular slit yielded the highest peak, followed by the semicircular slit and the triangular slit (Table 2). The backscattering peak heights for each type of slit were 31950.2 (1.077% of the photons detected) with the rectangular slit, 31504.2 (1.062%) with the triangular slit, and 31593.2 (1.065%) with the semicircular slit. The significances of the differences in the backscattering peaks were evaluated using the Chi-square test based on the histogram height. The Chi-square test over the histogram energy range

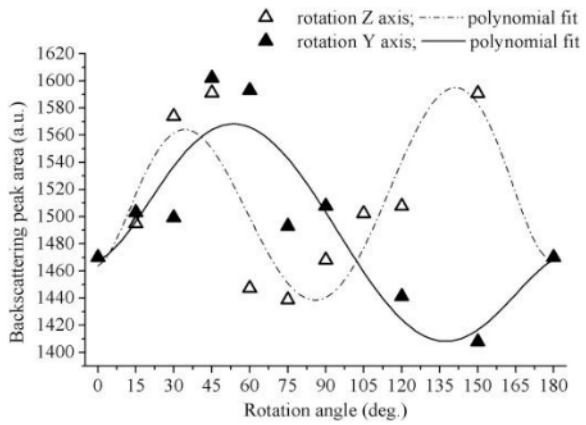

Fig. 11. Areas of the ^{137}Cs backscattering peaks with different rotations of the slit for the rectangular plate.

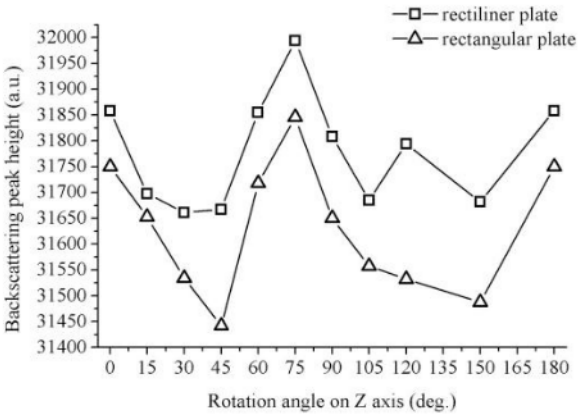

Fig. 12. Heights of the ^{137}Cs gamma backscattering peaks with different rotations of the slit on the Z-axis for rectilinear and rectangular plates.

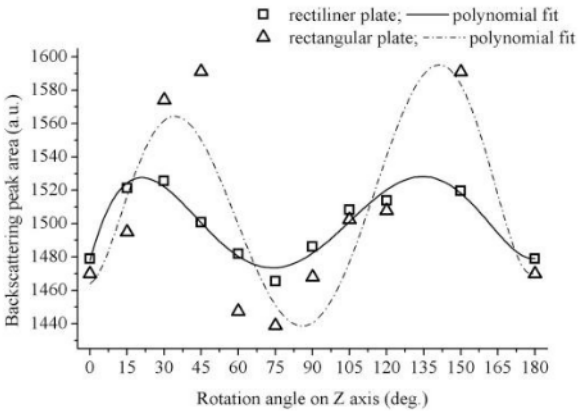

Fig. 13. Areas of the ^{137}Cs backscattering peaks with different rotations of the slit on the Z-axis for rectilinear and rectangular plates.

between 0.18 and 0.21 MeV (see Table 3) generated a critical value of 12.137 with 10 degrees of freedom and a confidence level of 72% (the critical value for the 95% confidence level was about 18.307). Thus, the slit shape had a small effect on the gamma backscattering peak curve in the energy distribution spectrum but the peaks were not significantly different from each other.

Moreover, the rotation of the slit influenced the backscattering peaks for the ^{137}Cs gamma-ray scattering energy received by the detector. This effect was demonstrated by the different heights of the backscattering peak due to the rotation of the slit on the Y-axis, as shown in Fig. 10 and Fig. 11.

According to the backscattering peak areas shown in Fig. 11, the effect of rotating the slit on the Y-axis can be described by the polynomial: $Y_{Y\_RECTA} = -3.87E\text{-}08x^5 + 1.8E\text{-}05x^4 - 0.002x^3 + 0.122x^2 + 0.597x + 1468$. In addition, the effect of rotating the slit on the Z-axis can be described by the polynomial: $Y_{Z\_RECTA} = 1.6E\text{-}09x^6 - 8.5E\text{-}07x^5 + 1.6E\text{-}04x^4 - 0.012x^3 + 0.339x^2 + 0.739x + 1464$. The coefficients of determination (R^2) for the fitted curves were about 0.800 and 0.753 for rotation on the Y-axis and Z-axis, respectively. These results indicate that rotating the slit affected the energy spectrum distribution detected for the gamma scattering, especially in the backscattering peak area.

The influence of the slit orientation was also investigated when the slit was rotated on the Z-axis or the axis perpendicular to the surface plane of the duralumin plate. Simulations were performed for

rectangular plates and rectilinear plates with the same volume and same slit size. Fig. 12 shows that the slit orientation significantly affected the height of the backscattering peak in the spectrum of the gamma energy distribution for ^{137}Cs.

According to the areas of the backscattering peak and the fitted polynomial curves, the effect of slit rotation on the Z-axis corresponded to a specific pattern, as shown in Fig. 13. The effect of changing the orientation was also determined for the rectilinear plate with the same thickness and volume as the rectangular plate, and with the same slit dimensions. According to polynomial interpolation, the effect can be described by the following equation: $Y_{Z\ RECTI} = 1.5E\text{-}10x^6 - 4.4E\text{-}08x^5 - 2.5E\text{-}06x^4 + 0.019x^3 - 0.187x^2 + 5.499x + 1478$.

The backscattering peak area results obtained with the rectilinear plate exhibited a similar pattern to those produced using the rectangular plate. The only difference was that the height of the backscattering peak area curve obtained for the rectangular plate was higher than that for the rectilinear plate. According to the coefficient of determination (R^2) values for the fitted polynomial curves comprising 0.953 for the rectilinear plate and 0.753 for the rectangular plate as well as the patterns formed, we can conclude that the orientation and rotation of the slit affected the area of the backscattering curve in the energy distribution for the gamma scattering spectrum obtained with the ^{137}Cs source.

5. Conclusions

In this study, we conducted simulations to investigate the effects of the presence of different slit types and their orientation on the backscattered peak curve obtained with a ^{137}Cs gamma source. The shape of the slit had a small effect on the peak of the backscattering curve. In addition, rotation of the slit changed the peak heights and specific patterns were generated in the backscattering peak area curve.

Declaration of competing interest

We declare that we do not have conflict interest of our paper with the title.

Acknowledgment

The authors are grateful to Mataram University for support through BLU (PNBP) research funding.

Appendix A. Supplementary data

Supplementary data to this article can be found online at https://doi.org/10.1016/j.apradiso.2019.108924.

References

Agostinelli, et al., 2003. GEANT4-a Simulation toolkit. Nucl. Instrum. Methods Phys. Res. 506, 250–303.
Almayahi, B.A., 2015. Backscattering factor measurements of gamma rays of the different thickness of pure concrete. J. Radiat. Res. Appl. Sci. 8, 389–392.
Aydın, A., 2018. Energy distributions of multiple backscattered photons in materials. Nucl. Sci. Tech. 29 (23), 1–6.
Ball, A.J., Solomon, C.J., Zarnecki, J.C., 1998. The response of gamma backscatter density gauges to spatial inhomogeneity - an extension of the single scattering model. Nucl. Instrum. Methods Phys. Res. B 140, 449–462.
Baldo, E.M., Appoloni, C.R., 2014. Inspection of reinforced concrete samples by Compton backscattering technique. Radiat. Phys. Chem. 95, 392–395.
Gurau, D., Rina, O., 2012. The examination of source distribution in a large sample by Monte Carlo simulation. Appl. Radiat. Isot. 70, 2141–2143.
Golgun, S.M., Sardari, D., Sadeghi, M., Mofrad, F.B., 2016. A novel method of combined detector model for gamma densitometer: theoretical calculation and MCNP4C simulation. Appl. Radiat. Isot. 118, 245–250.
Hosamani, M.M., Badiger, N.M., 2018. Determination of effective atomic number of composite materials using backscattered gamma photons – a novel method. Chem. Phys. Lett. 695, 94–98.
Kiran, K.U., Ravindraswami, K., Eshwarappa, K.M., Somashekarappa, H.M., 2015. Effective atomic number of selected construction materials using gamma backscattering technique. Ann. Nucl. Energy 85, 1077–1084.
Knoll, G.F., 1989. Radiation Detection and Measurement, second ed. John Wiley & Sons Inc, New York.
Nguyen, V.H., Chuong, H.D., Thanh, T.T., Tao, C.V., 2018. New method for processing gamma backscattering spectra to estimate saturation depth and to determine thickness of aluminum and steel materials. J. Radioanal. Nucl. Chem. 315, 293–298.
Peeples, J.L., Gardner, R.P., 2012. Monte Carlo simulation of the nonlinear full peak energy responses for gamma-ray scintillation detectors. Appl. Radiat. Isot. 70, 1058–1062.
Priyada, P., Ramar, R., Shivaramu, 2012. An improved Compton scattering method for determination of concentration of solutions. Appl. Radiat. Isot. 70, 2421–2427.
Priyada, P., Ramar, R., Shivaramu, 2013. Application of gamma ray scattering technique for non-destructive evaluation of voids in concrete. Appl. Radiat. Isot. 74, 13–22.
Sharma, R., Sharma, J.K., Kaur, T., Singh, T., Sharma, J., Singh, P.S., 2017. Experimental investigation of effective atomic numbers for some binary alloys. Nucl. Eng. Technol. 49, 1571–1574.
Shi, H.X., Chen, B.X., Li, T.Z., Yun, D., 2002. Precise Monte Carlo simulation of gamma-ray response functions for an NaI(Tl) detector. Appl. Radiat. Isot. 57, 517–524.
Tavakoli-Anbaran, H., Miri-Hakimabad, H., Izadi-Najafabadi, R., 2009. Optimization of a detector Collimator for Use in a gamma-ray backscattering Device for anti-personal landmines detection. J. Appl. Sci. 9, 1752–1757.
Tekin, U.A., Ozmutlu, E.N., Gurler, O., Yalcin, S., 2013. Monte Carlo analyses of multiple backscattering of gamma rays. J. Radioanal. Nucl. Chem. 295, 901–905.
Tondon, A., Singh, M., Sandhu, B.S., Singh, B., 2017. Nondestructive study of wood using the Compton scattering technique. Appl. Radiat. Isot. 129, 204–210.
Wirawan, R., Waris, A., Djamal, M., Gunawan, H., Kim, H.J., 2017. Monte Carlo modeling of gamma ray backscattering for crack identification in the aluminum alloy plate. IOP Conf. Ser.: J. Phys. Conf. Ser. 799, 012010.

B4

ORIGINALITY REPORT

14%	12%	13%	5%
SIMILARITY INDEX	INTERNET SOURCES	PUBLICATIONS	STUDENT PAPERS

PRIMARY SOURCES

1	coek.info Internet Source	2%
2	repositorio.ipen.br Internet Source	1%
3	P. Limkitjaroenporn, N. Wongdamnern, S. Kothan, J. Kaewkhao. "Density measurement of multi-layered material using gamma-ray transmission technique", Radiation Physics and Chemistry, 2021 Publication	1%
4	Huynh Dinh Chuong, Nguyen Duy Thong, Vo Hoang Nguyen, Le Hoang Minh et al. "Non-destructive evaluation of thickness of material plates through Compton back-scattering technique using Si(Li) detector", Radiation Physics and Chemistry, 2022 Publication	1%
5	cepsar.open.ac.uk Internet Source	1%
6	openaccess.sirnak.edu.tr Internet Source	1%

7	Hoang Duc Tam, Nguyen Thi My Le. "An improved method for liquid density measurement using NaI(Tl) detector and low-strength source", Journal of Radioanalytical and Nuclear Chemistry, 2018 Publication	1 %
8	Amandeep Sharma, Bhajan Singh, B.S. Sandhu. "A compton scattering technique for wood characteristics using FLUKA Monte Carlo code", Radiation Physics and Chemistry, 2021 Publication	1 %
9	docplayer.com.br Internet Source	1 %
10	Faidra Tzika. "Nondestructive Characterization of Radioactive Waste Drums by Gamma Spectrometry: A Monte Carlo Technique for Efficiency Calibration", Health Physics, 11/2007 Publication	1 %
11	Taranjot Kaur, Jeewan Sharma, Tejbir Singh. "Experimental measurement of effective atomic numbers and albedo factors for some alloys using the backscattering technique", Applied Radiation and Isotopes, 2020 Publication	1 %
12	iopscience.iop.org Internet Source	

		1 %
13	Rahadi Wirawan, Mitra Djamal, Abdul Waris, Gunawan Handayani, Hong Joo Kim. "Investigation of Incoherent Gamma-Ray Scattering Potential for the Fluid Density Measurement", Applied Mechanics and Materials, 2014 Publication	1 %
14	shahroodut.ac.ir Internet Source	1 %
15	www.itb.ac.id Internet Source	1 %
16	Li Zhang, Huawei Yu, Wenbao Jia. "A research on the effects of formation elements on the spatial distribution of D-D induced γ-ray source", Applied Radiation and Isotopes, 2019 Publication	1 %
17	upcommons.upc.edu Internet Source	1 %
18	D. Glavič-Cindro, M. Korun, B. Vodenik, B. Zorko. "Activity measurements of barrels filled with radioactive waste", Journal of Radioanalytical and Nuclear Chemistry, 2014 Publication	1 %
19	www.davidpublisher.com Internet Source	1 %

Exclude quotes	Off	Exclude matches	< 1%
Exclude bibliography	Off		

B4

GRADEMARK REPORT

FINAL GRADE

/0

GENERAL COMMENTS

Instructor

PAGE 1

PAGE 2

PAGE 3

PAGE 4

PAGE 5

PAGE 6

PAGE 7